Ship Airwake Sensitivities To Modeling Parameters

Jeremy Shipman*, Srinivasan Arunajatesan*, Christopher Menchini* and Neeraj Sinha†
Combustion Research and Flow Technology, Inc. (CRAFT Tech)
6210 Keller's Church Road, Pipersville, PA 18947

Accurate models for the prediction of ship airwake flowfields are critical to the development of realistic flight simulation tools for aircraft carrier launch and recovery operations. The accurate computation of the ship airwake can be very challenging due to the complexity of the ship geometry, the size of and difficulty in generating a suitable computational mesh, and the large range of length and time scales present in the unsteady flowfield. The present paper investigates the sensitivity of the airwake solution to several modeling parameters, including geometric complexity and the resolution of boundary layers, with the aim of determining the level of fidelity required to obtain an accurate solution. Results are compared to wind tunnel experimental measurements. The results of these studies show that, in general, a majority of the airwake flow features are characterized by bluff body shedding from the larger geometric entities that comprise the ship geometry. Depending on the requirements and intended use of the solution, a certain tradeoff can be reached between solution turn-around/grid generation time and solution accuracy.

I. Introduction

THE integration of aircraft with air capable ships is both a challenging and expensive task that carries an inherent risk to pilots. New V/STOL aircraft and rotorcraft in particular, such as the Joint Strike Fighter (JSF) and V-22, encounter unique challenges in performing takeoff and landing maneuvers during the course of shipboard operations due to the interaction of the propulsion-generated downwash with the unsteady airwake generated by the ship superstructure & deck. For such aircraft, wind-over-deck (WOD) launch and recovery envelopes must be developed, relating the compatibility of the specific aircraft with a specific ship at specific flight/wind conditions. This is currently accomplished through expensive, time-consuming sea trials for every aircraft and ship combination. Such trials entail numerous landing and takeoff operations, while incrementally (e.g., 5 knots speed or 15 degrees azimuth change) varying the WOD conditions. For multiple landing spot platforms, flight envelopes must be developed for each spot. The limits of the flight envelope are determined from the test pilot's subjective rating of the landing/take-off, taking into account factors such as pilot workload, flight control and power limitations of the aircraft, and ship motion. Safety is an additional issue of significant concern during these trials, due to the unknown response of the aircraft to the wind conditions. Modeling and simulation of the dynamic interface between the ship airwake environment and the aircraft can potentially reduce the cost and risk associated with these tests by providing a process for determining WOD performance envelopes via piloted flight simulation.[1,2,3] A crucial aspect involves the incorporation of physical models of the various subsystems into the flight simulator environment, including computational fluid dynamics (CFD) models of the ship airwake and aircraft propulsive flowfields.

Previous work by the authors presented the validation of a multi-element unstructured numerical framework for the computation of unsteady ship airwake flowfields.[4] Details on the extension of the CRUNCH CFD® code for the computation of low-speed unsteady flows was presented, along with validation studies entailing wind tunnel and full-scale airwake simulations.

The current paper presents a series of studies aimed at understanding the sensitivity of ship airwake simulations to a number of factors that affect the practical use of CFD as a tool for ship airwake prediction. Results are shown for a number unsteady CFD simulations that investigate the importance of such factors as geometric fidelity, i.e. the

43rd Aerospace Sciences Meeting and Exhibit, Jan. 10-13 2005, Reno, NV.

* Research Scientist, AIAA Member.
† Principal Scientist, AIAA Senior Member.

Report Documentation Page

Form Approved
OMB No. 0704-0188

1. REPORT DATE	2. REPORT TYPE	3. DATES COVERED
2005		**00-00-2005 to 00-00-2005**

4. TITLE AND SUBTITLE	5a. CONTRACT NUMBER
Ship Airwake Sensitivities to Modeling Parameters	5b. GRANT NUMBER
	5c. PROGRAM ELEMENT NUMBER
6. AUTHOR(S)	5d. PROJECT NUMBER
	5e. TASK NUMBER
	5f. WORK UNIT NUMBER
7. PERFORMING ORGANIZATION NAME(S) AND ADDRESS(ES) **Combustion Research and Flow Technology Inc (CRAFT Tech),6210 Keller's Church Road,Pipersville,PA,18947**	8. PERFORMING ORGANIZATION REPORT NUMBER
9. SPONSORING/MONITORING AGENCY NAME(S) AND ADDRESS(ES)	10. SPONSOR/MONITOR'S ACRONYM(S)
	11. SPONSOR/MONITOR'S REPORT NUMBER(S)

12. DISTRIBUTION/AVAILABILITY STATEMENT
Approved for public release; distribution unlimited

13. SUPPLEMENTARY NOTES
The original document contains color images.

14. ABSTRACT

15. SUBJECT TERMS

16. SECURITY CLASSIFICATION OF:			17. LIMITATION OF ABSTRACT	18. NUMBER OF PAGES	19a. NAME OF RESPONSIBLE PERSON
a. REPORT	b. ABSTRACT	c. THIS PAGE			
unclassified	**unclassified**	**unclassified**		**14**	

level of geometric complexity of hull and superstructure features included in the model, and the fidelity of the flowfield model, such as the inclusion or exclusion of viscous boundary layers on the ship surfaces. While these factors can have an effect on the accuracy of the solution, they also have a large impact on the cost of the simulation, in both grid generation effort and CPU time to obtain the solution. Depending on the ship/aircraft configuration and the aircraft flight path locations, i.e. in the wake of the superstructure or along the deck edge for helicopter landing spots, these various modeling parameters may or may not be important.

The sensitivity of the airwake computation to the geometric complexity of the ship model is investigated for simulations of CVN-class aircraft carrier models having superstructure configurations with varying degrees of detail. Results are presented for wind tunnel scale simulations of the CVN model. The solutions from the wind tunnel scale cases are compared to wind tunnel measurements of the ship model airwake. Additional studies are presented that investigate the sensitivity of the airwake solution to the resolution or exclusion of viscous boundary layers on the hull and superstructure surfaces. Isolated studies on both hull and superstructure components of a ship geometry, as well as the entire CVN ship geometry are presented. The results of these calculations are also compared to wind tunnel measurements.

II. Sensitivity to Geometric Representation

The geometry of air capable ships can be extremely complex if one considers all the details of features such as hull appendages, masts, and superstructure details. For computational simulations, the level of complexity that is included in the geometric model directly affects the expense and turn-around time of the calculation, and can have an impact on the accuracy of the solution. While it is not feasible to include every detail of the ship geometry, advances in unstructured grid generation tools make it possible to include a greater degree of complexity in the CFD mesh. However, for CFD to be a practical tool for developing WOD performance envelopes, a trade-off must be reached between the competing requirements of solution turn-around/grid generation time and solution accuracy.

In order to study these issues, wind tunnel scale simulations were performed involving simple and complex representations of a CVN-76 superstructure mated to a generic CVN class hull geometry. The simulations replicate wind tunnel tests performed at NAVSEA, Carderock Division [5,6]. The wind tunnel data was provided to CRAFT Tech by NAVAIR.

A. Wind Tunnel Scale CVN Studies: Detailed vs. Simple Island Configuration

A photograph of the various wind tunnel configurations used in the Carderock test is shown in Figure 1. The model geometry consists of an interchangeable superstructure, or island, shape mounted to a hull shape representative of a CVN class carrier. The wind tunnel model is 1/144th scale. The island models depicted in the inset of Figure 1 correspond to (from left to right) a simplified CVN-76, a complex CVN-76, and a CVN-73 shape. Results from the wind tunnel runs made using the simple and complex CVN-76 superstructure models are of interest to this study.

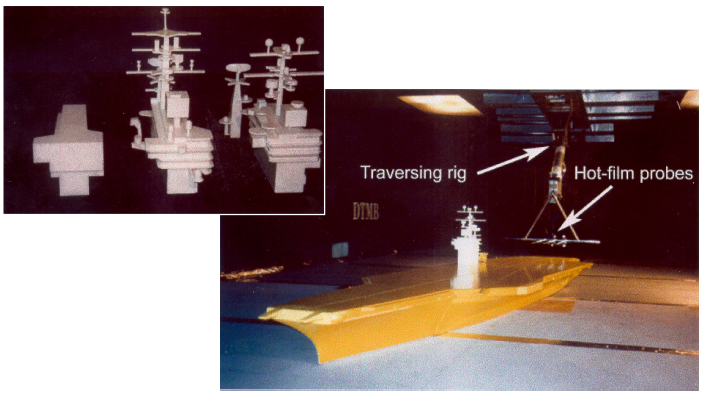

Figure 1. Photograph of the wind tunnel geometric configurations.

The model geometry used in the simulations is shown in Figure 2, illustrating the wind tunnel duct configuration and a close up of the ship model. An unstructured computational grid was constructed from CAD representations of the hull and simple/complex island wind tunnel models using Gridgen[7]. A high quality mesh was created on the ship surfaces, with good resolution along the edges of the hull and island surface features. For this study, prism layers

were not extruded from the ship surfaces to resolve the viscous boundary layers. The complex island model, itself a simplification of the actual CVN-76 geometry, is nevertheless a reasonable representation of the major features of the island superstructure. The extremely complicated shape (from a grid generation point of view) includes multiple mast, antenna, and structural features representative of the actual configuration. Figure 3 illustrates details of the surface mesh for the hull and the two island configurations. A tetrahedral mesh was created in the test section portion of the wind tunnel geometry. The resolution of this mesh was controlled so that a finer spacing of grid points was placed in the key areas of the wake behind the island and hull, along the landing trajectory, and around the deck edges. Hexahedral blocks using stretched, anisotropic cells in the inlet and outlet ducts complete the wind tunnel grid. A summary of the relevant grid statistics for the complex and simple island configurations is listed in Table 1. All other parameters being the same, the reduced complexity of the simple island shape results in a smaller grid size as compared to the complex island configuration.

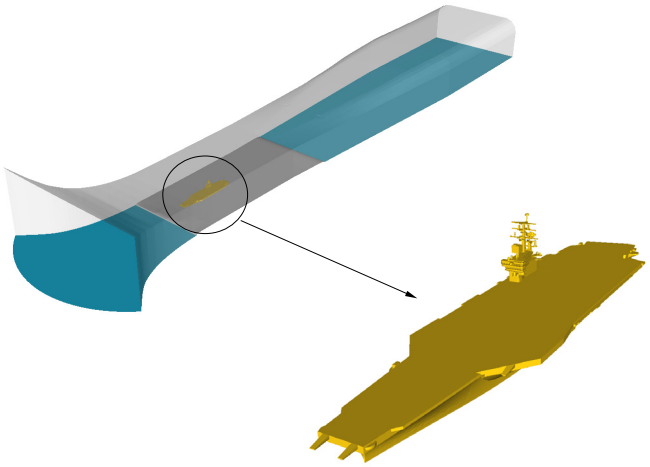

Figure 2. Configuration of the simulation geometry.

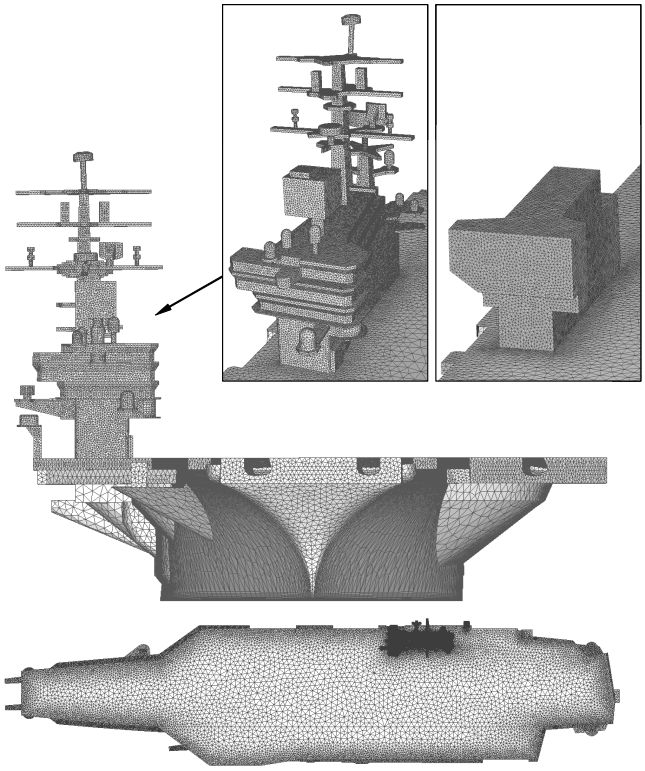

Figure 3. Details of the CVN-76 surface mesh.

Table I. Grid statistics for the two configurations.

Grid Size Statistics	**Complex Island Grid**	**Simple Island Grid**
Number of vertices	1,243,139	825,549
Number of tetrahedra	6,908,459	4,484,610
Number of Pyramids	960	960
Number of hexahedra	48,000	48,000
Number of boundary faces	200,056	131,380

The simulations correspond to wind tunnel conditions that represent a 0°, 25 knot WOD. The grid was partitioned over 64 processors and a time-accurate simulation was performed using CRUNCH CFD® spanning a time interval of 1.4 seconds for each of the cases. A time step of 0.0002 seconds was specified, thus 7000 iterations were required after a startup initialization period of about 1000 to 2000 iterations. A snapshot of the solution for both cases is illustrated in Figure 4, showing isosurfaces of vorticity colored by velocity magnitude. The plots illustrate the shedding and subsequent roll-up of deck edge vortices from the bow, and the unsteady fluctuations of the airwake particularly in the region behind the superstructure. While the solutions look identical for the majority of the flowfield, there are significant differences between the simple and complex island configurations evident in the structure of the island wake. The simple configuration shows larger scale shedding phenomena with higher velocities, whereas the many features protruding from the complex island act to break up the large vortices into smaller scale, higher frequency structures.

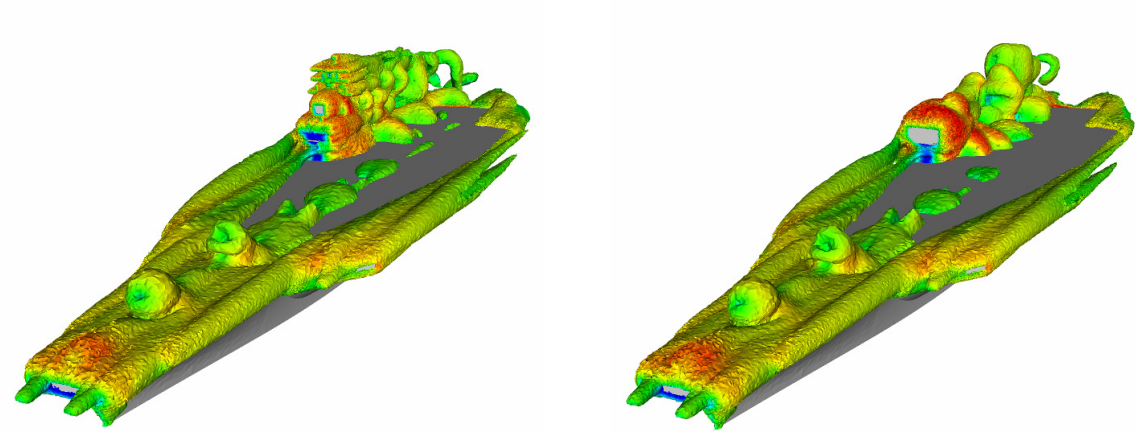

(*a*) complex island (*b*) simple island

Figure 4. Isosurface of vorticity showing a comparison of the solutions for the (*a*) complex and (*b*) simple island configurations.

Mean and rms velocity data from the simulations were calculated for a number of points in the wake region corresponding to the data probe locations of the wind tunnel measurements shown in Figure 5. The measurements were taken at points along an ideal flight path extending from the touch down point, and aligned with the angled deck (9° with respect to the keel line). A wake survey recorded additional measurements in a broader wake region downstream of the ship model, also aligned with the angled deck. Figure 5 illustrates the locations of the probe points for the flight path (red) and the wake survey (blue) in relation to the CVN-76 complex island model. The comparisons presented here are for a subset of 15 points along the center of the flight path line extending 1350 feet (in full scale units) behind the touchdown point on the deck.

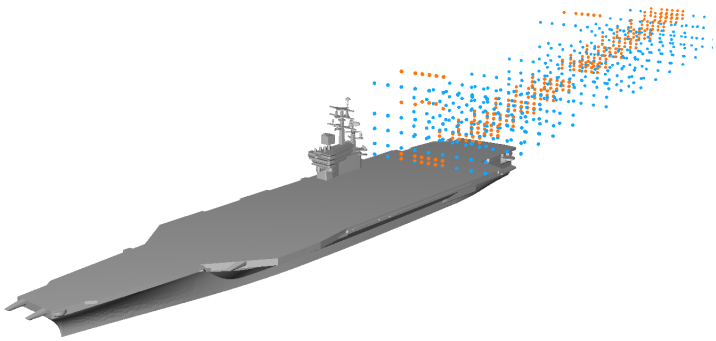

Figure 5. Diagram of data probe points.

The mean and rms velocity results for the 15 points in the flight path are plotted against the wind tunnel measurements in Figures 6 and 7. The points are plotted as a function of the downstream distance (corresponding full scale) from the touch down point on the angled deck. Figure 6 shows the comparison of results from both cases with the wind tunnel measurements for mean u, v, and w velocities. Both the CFD results and wind tunnel measurements show a degree of difference in the mean velocities between the simple and complex configurations. The difference is greatest starting at a distance of 400 ft, several hundred feet aft of the ship in the wake of the island. In general, the CFD results tend to over predict the mean velocity magnitude, which could be due to the assumption of symmetry along the mid plane of the wind tunnel (assuming blockage below the model plate from

support structures equals that of the ship model) and the slotted test section walls present in the Carderock wind tunnel but not modeled in the simulations. The CFD results for both configurations over predict a down draft from the rear of the hull, as shown by the mean w velocity at a location of about 200 ft behind the touchdown point, which corresponds to the ramp on the back edge of the deck.

Figure 7 shows plots of the rms u, v, and w velocities with respect to the wind tunnel measurements. The measurements show higher rms velocities for the simple configuration to about 400 ft, from which point the rms velocities for the complex configuration are higher. The CFD results capture this trend, as well. However, for the simple island configuration, the rms velocities for all three components are over predicted at the 200 ft location, corresponding to the deck ramp.

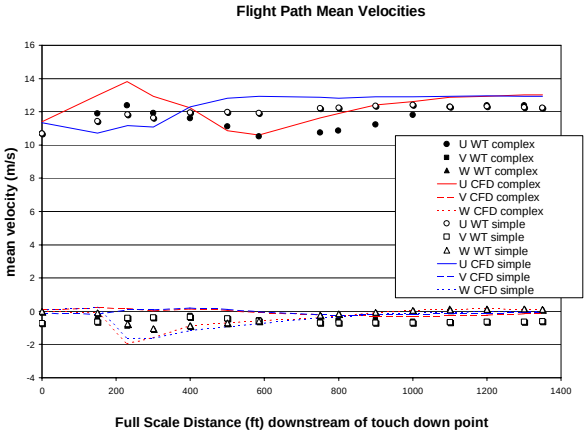

Figure 6. Comparison with wind tunnel measurements along the flight path for the mean velocities.

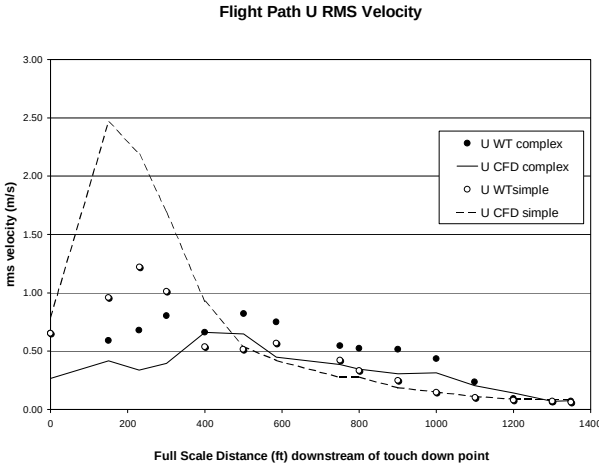

(a)

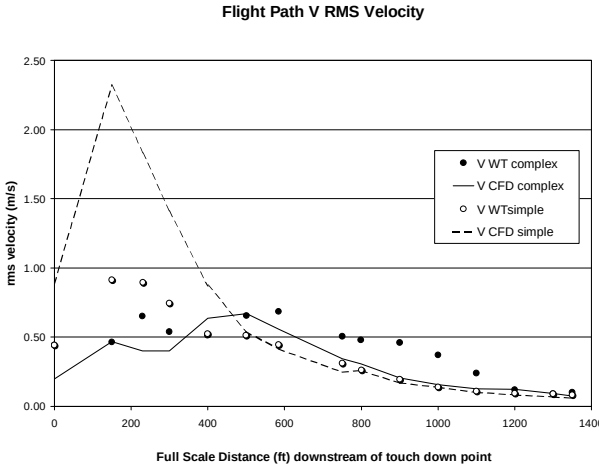

(b)

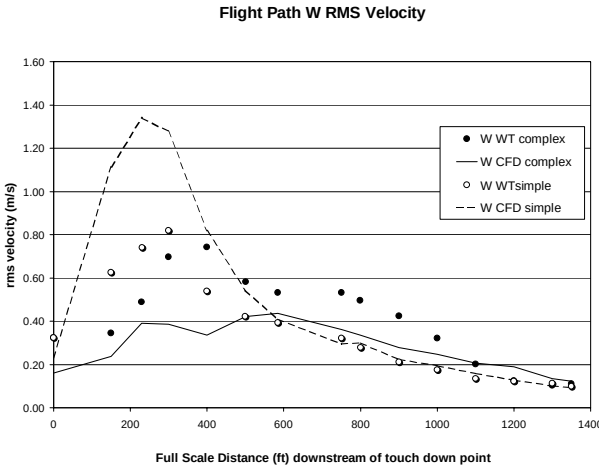

(c)

Figure 7. Comparison with wind tunnel measurements along the flight path for the u, v, and w rms velocities.

The results of these simulations show that although the majority of the flowfield around the ship is not sensitive to the level of geometric complexity of the island shape, there are significant differences along specific sections of the landing flight path that traverse the island wake. Therefore, depending on the particular landing scenerios of interest and factors such as the wind angle, the increased cost of including the finer geometric detail must be weighed against the fidelity required for the intended use of the data. A significant cost savings is realized by neglecting the finer details of the island shape, as shown in the grid size statistics in Table I. The complex island grid is roughly 1.5 times larger due to the increased resolution required to resolve the many intricate details of the masts and antenna features. With the grid partitioned over the same number of processors, the smaller grid size for the simple island case translates to a corresponding savings in CPU time. Because the two simulations were not run on the same computer system, an exact comparison of CPU times is not available. In addition to the simulation cost savings due to grid size, the reduction in grid generation effort for the simple island case is significant. A considerable amount of time was required in the preprocessing steps of CAD model cleanup and surface meshing for the complex island configuration. If the simulation is to include boundary layer resolution, as discussed in the following section, the inclusion of the complex geometric features further complicates the grid generation process.

III. Flowfield Modeling Sensitivities

In the following sections, results are presented for studies investigating the sensitivity of the airwake solution to the inclusion or exclusion of viscous boundary layers in the flowfield model. In previous work by the authors, a series of full scale cases involving a simplified LHA ship geometry indicated that a large part of the ship airwake dynamics is driven by bluff body shedding, and that applying inviscid walls to some or all of the ship surfaces might be sufficient to capture the dominant features of the airwake flowfield. Presented here are more detailed studies that were performed to investigate the impact on the accuracy of the airwake solution of neglecting boundary layers. The following three studies were performed, investigating the boundary layer sensitivities of the airwake solution to the hull and deck boundary layers, finer scale superstructure components such as mast and antenna features, and the entire CVN-76 ship model:

1. Ship Deck Boundary Layer Study. Results are presented for a series of studies looking at the importance to the ship airwake flowfield of boundary layers on the large scale structures of the ship hull and deck. Simulations were run with and without boundary layers for a ship deck and hull geometry. These studies isolate the importance of resolving the boundary layer on the flight deck surface as opposed to other regions of the ship geometry such as the superstructure surfaces.
2. Ship Mast Boundary Layer Study. Results are presented for simulations with and without boundary layers on a complex ship mast geometry to investigate the importance of resolving the boundary layer on the smaller, more intricate features found on the superstructure, or island portion of the ship. The results are compared to wind tunnel measurements of the same configuration provided by NAVAIR.
3. Entire Ship Model Study. Results are presented for simulations of the CVN-76 wind tunnel configuration described in previous sections. For these cases, the complex CVN-76 island configuration is used. The results are compared to the Carderock wind tunnel measurements for the complex island model.

A. Ship Deck Boundary Layer studies

To investigate the importance of the ship deck boundary layer, two meshes were constructed with Gridgen for a simplified full scale LHA hull and deck geometry with the island removed. Both grids were constructed from the same triangulated surface grid with a spacing of about one foot along all the deck edges, with the exception of a denser surface spacing on the bow. For the ship length of 840 feet, the boundary layer thickness based on

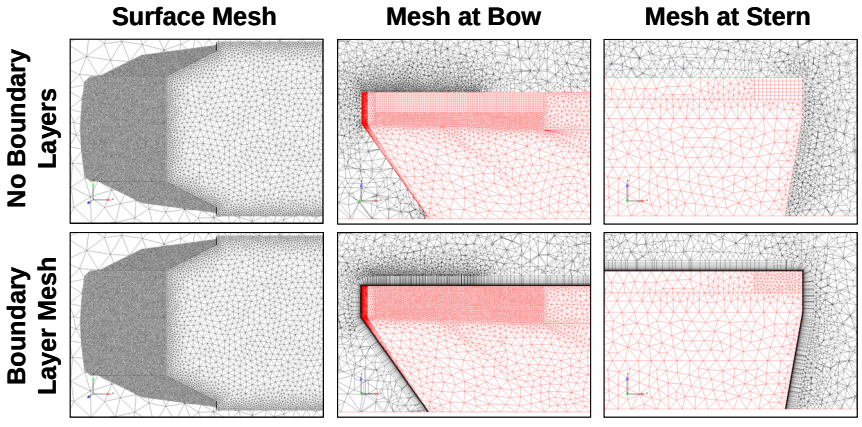

Figure 8. Comparison of surface mesh for the inviscid and viscous grids.

correlations is about one foot. The viscous mesh was constructed by extruding prism layers to a height of approximately 5 ft, well encompassing the predicted boundary layer thickness. The tetrahedral volume meshes for both grids are nearly identical, using the same tetrahedral size factor and identical outer domains. A comparison of the surface and volume meshes for both grids is shown in Figure 8.

Three cases were run with the two grids: (1) no boundary layer mesh with slip wall boundaries, (2) boundary layer mesh with slip wall boundaries, and (3) boundary layer mesh with no-slip wall boundaries. The later two cases were meant to test the effects of the viscous boundary condition as opposed to that of the increased boundary layer resolution alone. The results are similar for all three cases. Figure 9 shows a comparison of the mean u velocity component for the y = 0 plane, corresponding to the centerline plane of the hull geometry (the y axis is oriented along the span of the deck, positive to port). All three cases show a similar recirculation region at the bow which is important to the shedding characteristics of the airwake. Slight differences are seen in the wake region of the rear of the hull, which could be important depending on the approach path of landing aircraft. Mean velocity comparisons were made for a number of axial locations along the length of the hull. Shown in Figure 10 is the comparison for an axial location 50 feet from the bow. This location is near the bow within the refined surface region shown in the surface mesh plot of Figure 8. The plots show almost identical features with the exception of a slightly better resolved deck edge rollup, which could be important for rotary wing aircraft landing spots along the deck edge. Unsteady velocities and fft's are plotted for the three cases at two axial locations 557 and 632 feet from the bow in Figure 11. The plots show a similar range of amplitude and frequency in the fluctuations for both of the axial locations, which correspond to about 2/3 and 3/4 of the hull length.

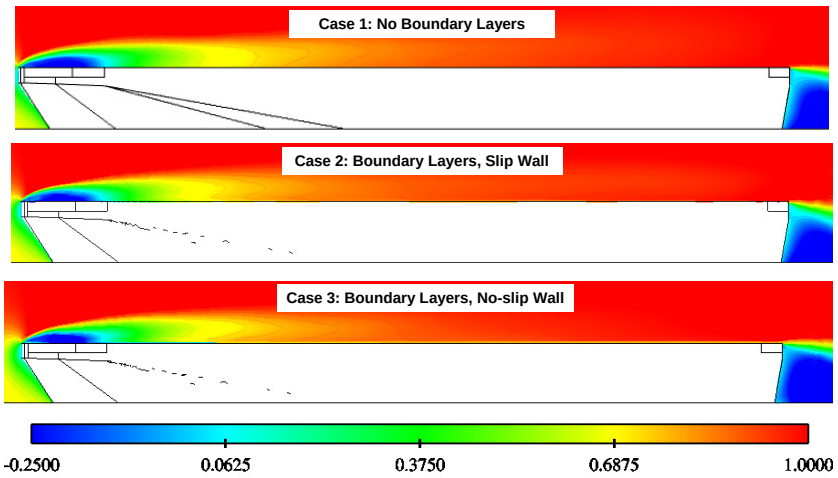

Figure 9. Comparison of mean u velocity at the centerline plane.

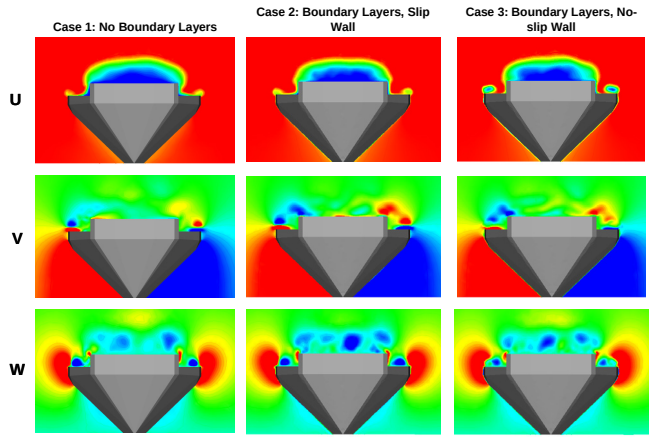

Figure 10. Mean u, v, and w velocity for an axial location near the bow.

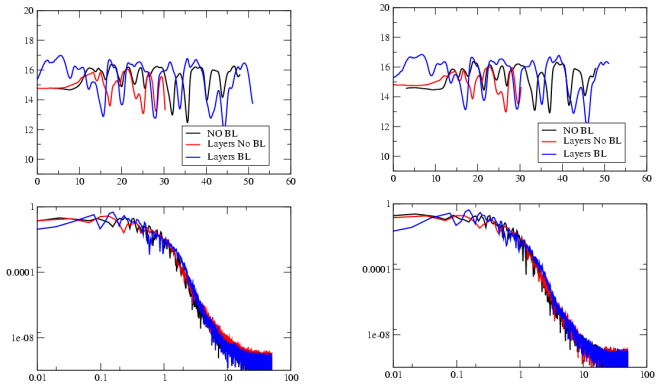

Figure 11. Unsteady velocity and FFT at two x locations near the stern.

B. Ship Mast Boundary Layer Studies

Three cases were run to determine the importance of resolving the boundary layers on geometrically complex ship features such as mast and antenna structures. Grids without boundary layers, with minimal boundary layers, and with an improved boundary layer extrusion were constructed with Gridgen[7] for a complex ship mast geometry for which wind tunnel data is available. A photograph of the wind tunnel model is shown in Figure 12. The geometry used to construct the grids includes the wind tunnel mounting plate, the ship mast structure, the wind tunnel walls, and the mounting bolts that protrude from the plate. The surface definition was provided in the IGES format, which required extensive clean up before surface grids could be made. Several of the diagonal elements were removed from the truss structure in order to avoid acute corners that would complicate prism extrusion for the viscous mesh. All three grids included a high-quality boundary layer mesh for the flat mounting plate and model base plate, while prism layers were extruded on the mast surfaces for the boundary layer grids only. For the first-pass boundary layer grid, several highly concave corners in the geometry limited the prism layer extrusion on the mast surfaces to five layers, resulting in a relatively thin boundary layer mesh on the mast surfaces. An additional case was run with an improved second-pass boundary layer grid, in which a high quality prism layer extrusion was obtained. This was made possible by conditioning the geometry with CAD tools to remove many of the acute corners that limited the original extrusion process by chamfering, or adding fillets, to the corner regions of the truss elements. The small fillets that were added in these locations enabled a more refined wall clustering and a greater number of prism layers that extended further into the volume. In addition to the increased resolution, the improved mesh allowed for a smoother transition in cell size from the prism to tetrahedral regions of the volume grid.

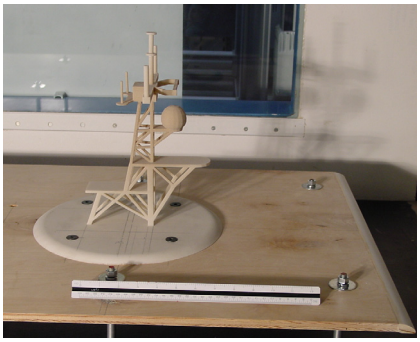

Figure 12. Ship mast wind tunnel model geometry.

Figure 13 shows details of the surface grid, as well as the plate and first-pass mast boundary layer grids. The same parameters were used to construct the tetrahedral volume meshes for the three cases, resulting in similar volume grids. The Gridgen "baffle" feature was used to control the grid resolution in a region containing the wake flowfield out to a distance of three feet behind the model. Wind tunnel measurements were taken at three planes: 12, 23.8, and 35.9 inches behind the model.

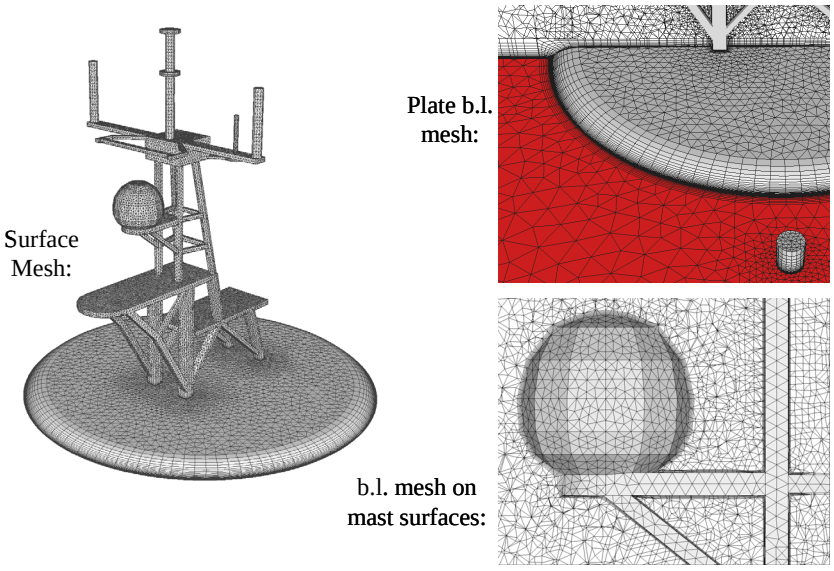

Figure 13. Detail of the surface and boundary layer grids.

The three cases were run for 12,300 iterations at a time step of 0.0002 seconds, resulting in a simulation time interval of about 2.5 seconds. Mean u, v, and w velocity plots of the results are shown in Figure 14 for the centerline plane and a horizontal plane parallel to the base plate that intersects the large block shape on the top of the mast. The plots show a very close comparison for the mean velocities in the wake region, showing very little impact of the prism layer mesh and the no-slip boundary applied in the viscous mesh.

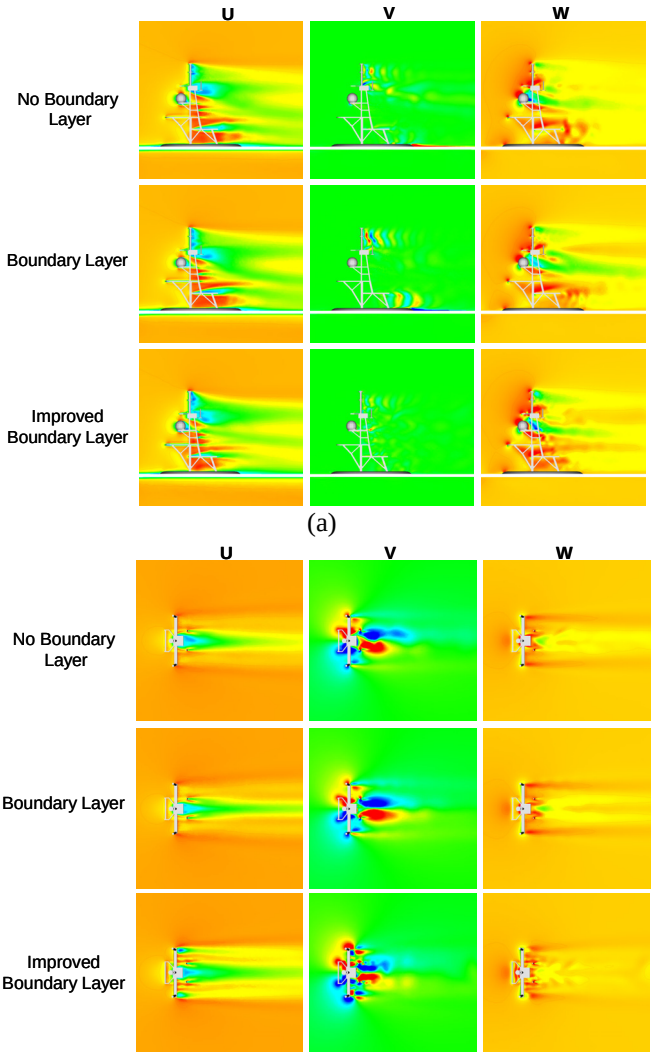

Figure 14. Comparison of mean velocities for (*a*) the centerline plane, and (*b*) a horizontal plane 8.5 inches from the base plate.

Mean and rms velocities were recorded for a set of probe points distributed in the wake of the mast model as shown in Figure 15. The points correspond to the location of anemometer measurements in the wind tunnel test, distributed in three planes, 1, 2, and 3 feet behind the model. The Mean velocity results for the three cases are compared to the wind tunnel measurements at each respective plane of points and plotted versus probe point number in Figure 16. The rms velocities are plotted against the wind tunnel measurements in Figure 17. In this plot, the results are plotted for a subset of 40 probe points per plane: points 1 to 40 are located in the 1 ft plane, points 41 to 80 are located in the 2 ft plane, and points 81 to 120 are located in the 3 ft plane.

In general, the results of all three cases

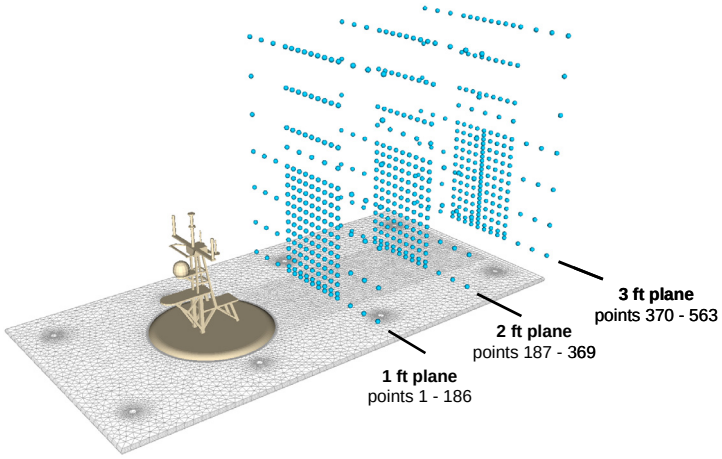

Figure 15. Ship mast data probe locations.

compare fairly well with the wind tunnel measurements. However, the comparisons highlight in more detail some of the differences between the two cases, as well as a few differences between the numerical and experimental results. While the improved boundary layer case tends to match closer to the measured velocities for most of the points, for some points, the case with no boundary layers is closer. The improved boundary layer case exhibits higher rms fluctuations. The first-pass boundary layer mesh is consistently further from the experimental measurements as compared to the other two cases.

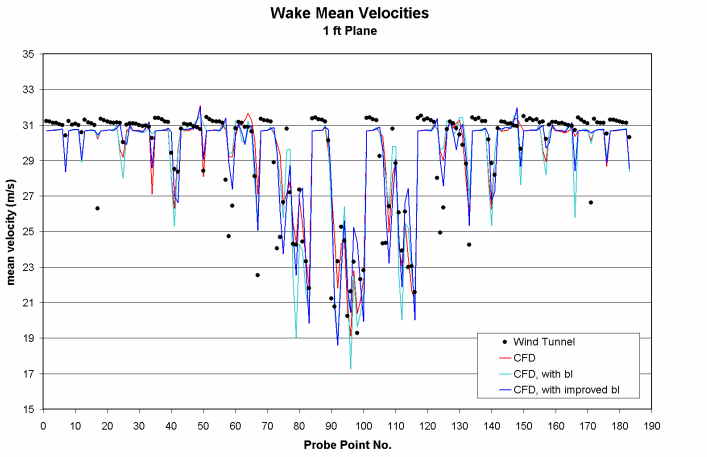

(a)

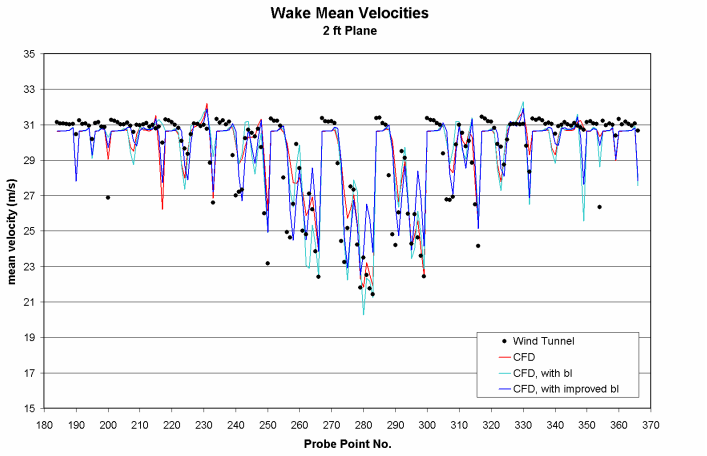

(b)

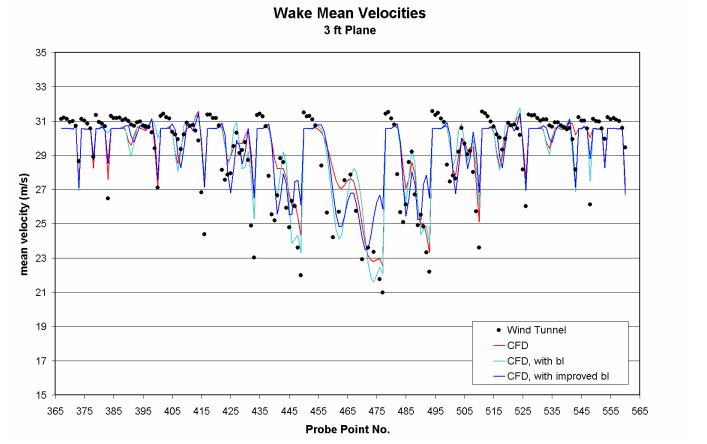

(c)

Figure 16. Comparison of mean velocities in the wake with experimental measurements for (*a*) the 1 ft plane, (*b*) the 2 ft plane, and (*c*) the 3 ft plane of probe points.

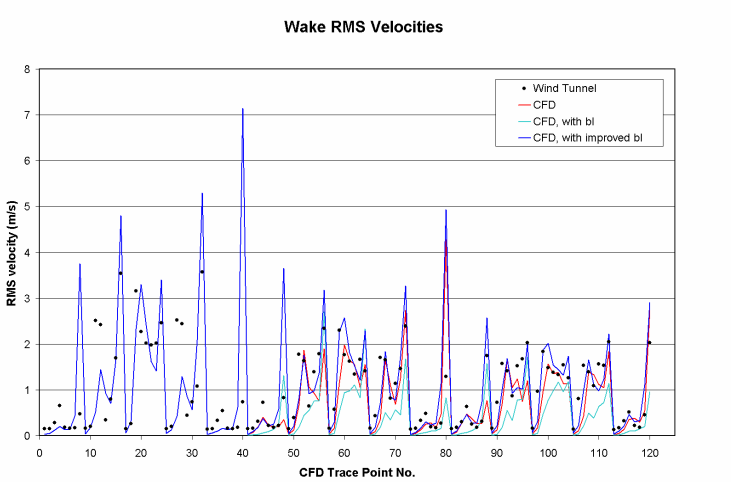

Figure 17. Comparison of rms velocities in the wake with experimental measurements.

C. Full Ship Geometry Boundary Layer Studies

An additional simulation was performed for the 1/144 scale CVN-76 wind tunnel case described in the geometric complexity studies, in which prism layers were extruded from the ship hull and island surfaces together. The results of this case were compared with the previously described no-boundary-layer wind tunnel scale CVN-76 simulation and to the experimental measurements. A fairly thick prism mesh was obtained, with seven layers extruded from the surface before being constrained by several corners on the hull geometry. The complex island geometry was slightly modified in a few locations to eliminate highly concave corners or degenerate surface normals, but the majority of the geometric complexity was preserved. The addition of prism layers on all the ship surfaces resulted in a significantly larger grid size, as listed in Table II. The CFD results were recorded at a subset of the measurement points depicted in Figure 5: 16 points per downstream plane and 15 points along the center of the flight path line.

The results are plotted against the wind tunnel measurements in Figures 18 through 21. The mean u, v, and w velocity components for the flight path and wake points are plotted in Figures 18 and 19, respectively, as a function of the location downstream of the touchdown point (in full-scale units). The mean velocities for the CFD results match the wind tunnel data fairly well, although the means are somewhat elevated for all the points. This is most likely due to the blockage of the ship model in the tunnel and the assumption of symmetry above and below the plate on which the model is mounted. In the wind tunnel runs, the test section walls were vented to accommodate the blockage of the model, which is not accounted for in the CFD model. For the mean u velocity, the case without boundary layers matches the measurements slightly better. In the case of the mean w velocity, neglecting the boundary layer tends to overpredict the downdraft at the rear deck edge ramp, as noted by the increased negative magnitude of the w velocity component around the 200 ft mark of the flight path.

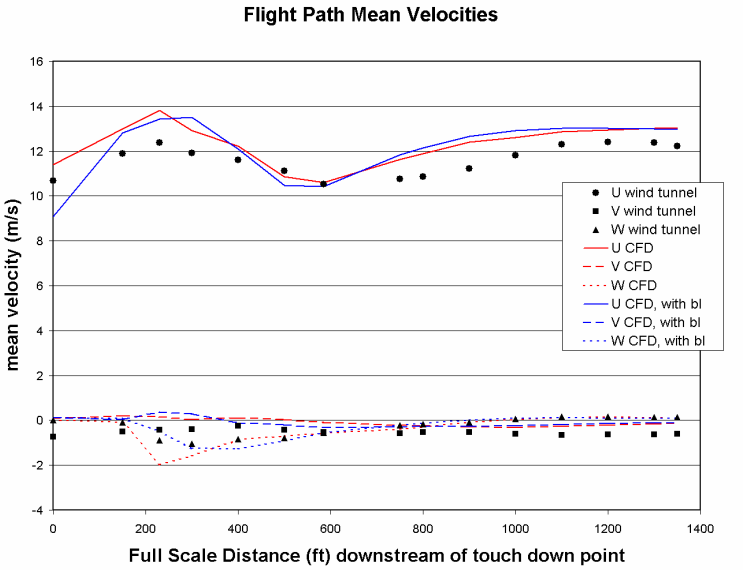

Figure 18. Comparison of the mean velocity results with wind tunnel measurements along the flight path.

The rms u, v, and w velocity components for the wake are plotted in Figure 20 as a function of the probe point number, where the rms velocities for each case are shown on a separate plot for clarity. The spike in rms velocities every 16 points correspond to the wake points that are located directly behind the ship model. Both cases show a similar drop off in rms velocities for the higher number points (further downstream) as the grid resolution in the wake starts to relax. Otherwise, the results for both cases are very close to the experimental measurements. The boundary layer case shows only very slightly higher rms values. The time histories for the u velocity component are plotted for the two cases against the wind tunnel measurements for the first three points along the flight path in Figure 21.

The results of this study show that, as with the ship mast and deck simulations, resolving the boundary layer for the hull and island surfaces has a minimal effect on the dominant features of the wake flowfield. The increased cost simulation time and grid generation effort that results by resolving the boundary layers must be weighed against the fidelity required for the intended accuracy of the solution. While there is a small effect, the case without boundary layers comes very close to and sometimes better than the boundary layer case in matching the wind tunnel data at the probe point locations. If the fidelity requirements allow neglecting the boundary layers, considerable cost savings can be achieved as shown in the grid statistics listed in Table II. The grid size is doubled with the addition of the boundary layer extrusion. Partitioned over the same number of processors, the CPU time per iteration for the boundary layer case is also almost doubled: 48 seconds per iteration for the case without boundary layers compared with 82 seconds per iteration for the boundary layer case.

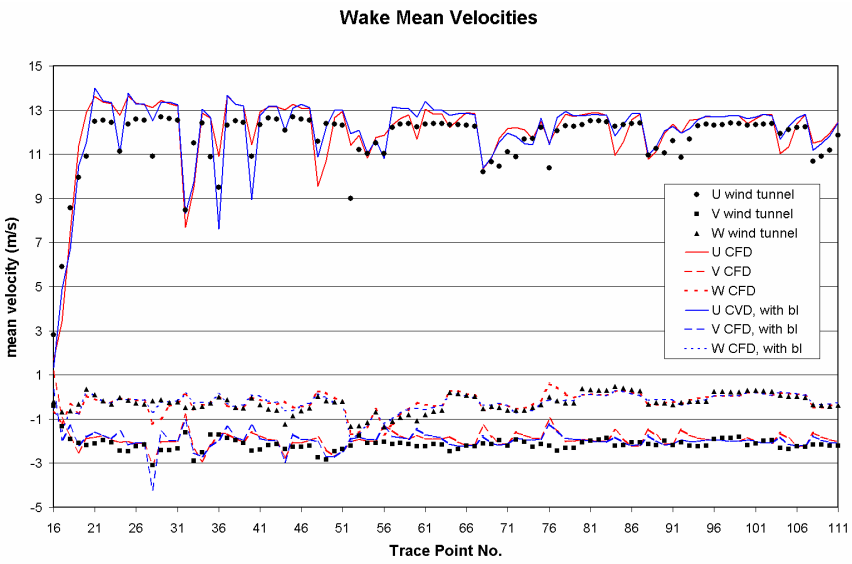

Figure 19. Comparison of the mean velocity results with wind tunnel measurements in the ship airwake.

Table II. Grid statistics for the two configurations.

Grid Size Statistics	No Boundary Layer Grid	Boundary Layer Grid
Number of vertices	1,243,139	2,382,348
Number of tetrahedra	6,908,459	9,090,608
Number of prisms	0	1,511,886
Number of Pyramids	960	960
Number of hexahedra	48,000	48,000

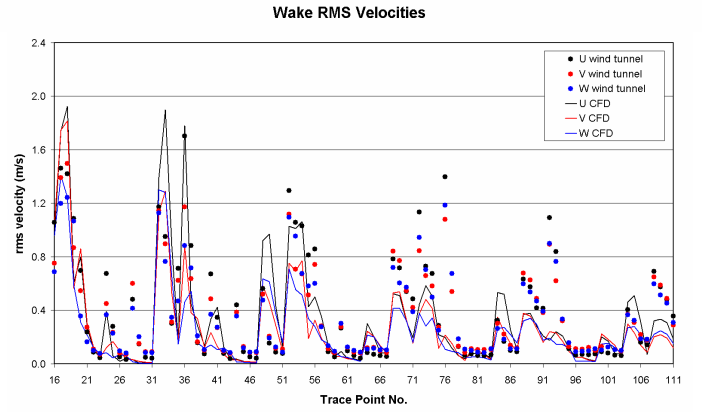

(a)

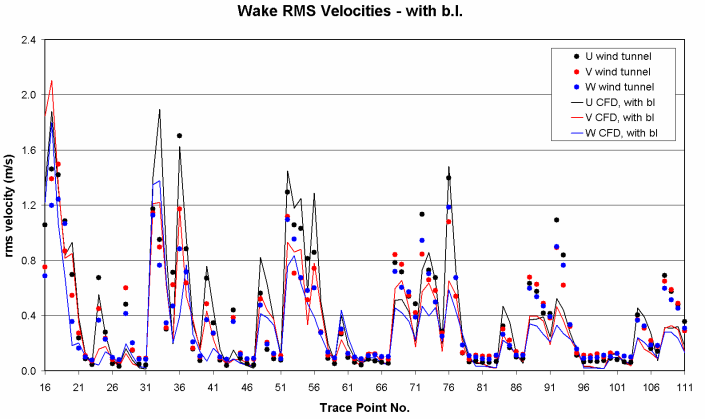

(b)

Figure 20. Comparison of rms velocities with wind tunnel measurements in the ship airwake for (a) without boundary layers, and (b) with boundary layers.

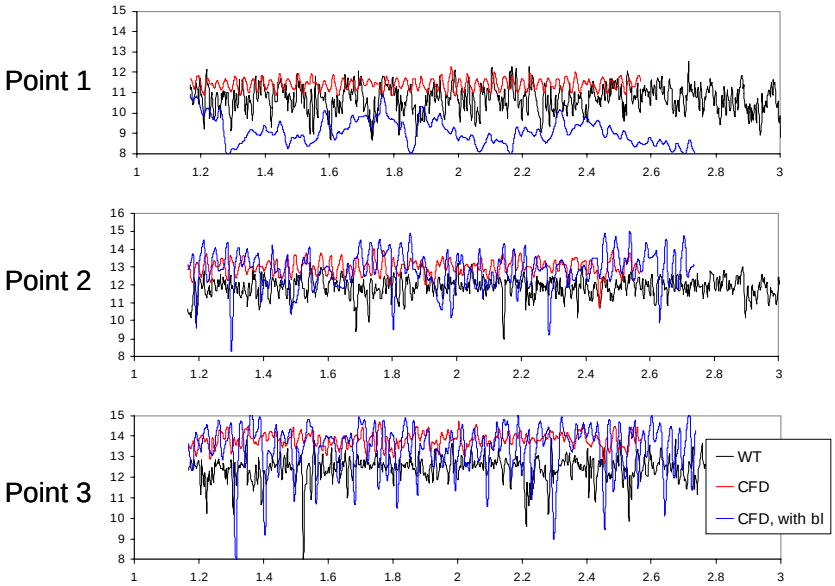

Figure 21. Time histories (x axis in seconds) of the velocity components for the first three points in the flight path line.

IV. Conclusions

Results have been presented for a series of studies using the CRUNCH CFD® unstructured solver with the aim of understanding the sensitivities of a ship airwake solution to various modeling parameters such as the geometric complexity and the resolution of boundary layers on the ship surfaces. The significance of these factors on the practicality of using CFD for WOD envelope predictions is important in that they affect not only the accuracy of the simulation, but the cost of the simulation as well, both in grid generation effort and CPU time. The results of these studies show that while a majority of the airwake dynamics is characterized by bluff body shedding from the main components of the ship geometry, the accuracy of the solution does depend on the fidelity to which the simulation parameters studied here are modeled. A tradeoff therefore exists between the opportunity to lower the cost of the simulation and the required fidelity of the solution based on the intended use of the simulation results.

Wind tunnel scale simulations have been presented involving simple and complex representations of an aircraft carrier geometry to study the sensitivity of the airwake solution to the modeled complexity of the superstructure/island shape. The solutions have been compared to wind tunnel velocity measurements of the ship's wake for each of the configurations. The results show that while the majority of the flowfield is not sensitive to the complexity of the island shape, there are significant differences in the immediate vicinity of the island wake. For a fixed wing aircraft landing on the angled deck of the carrier, the landing flight path takes it through this affected region, and is therefore an important consideration. Conversely, significant cost savings are realized by neglecting the finer details of the island shape, due to the large portion of the grid points required to resolve the many intricate details of the masts and antenna features.

An additional series of simulations has been presented investigating the sensitivity of the airwake solution to the resolution of boundary layers on ship surfaces. Three studies have been performed focusing on the resolution of the deck boundary layers, ship mast boundary layers, and boundary layers on a full CVN geometry. In the case of the ship mast and full ship studies, the solutions have been compared to wind tunnel measurements. The general conclusions are that a majority of the airwake flowfield is characterized by bluff body shedding, and that only in localized regions such as near the deck edge or immediately downstream of mast structures does the resolution of the boundary layers have a considerable impact on the solution accuracy. Large savings in simulation cost due to the decreased grid size and grid generation effort is achieved by neglecting the boundary layers. Thus, depending on the particular landing scenarios of interest and the required fidelity based on the intended use of the data, the boundary layer modeling effort and cost can be reduced, allowing a more practical use of CFD as a tool for predicting WOD envelopes.

Acknowledgments

Funding for this work has been provided by a Navy Phase II SBIR, Contract number N68335-03-C-0114, from NAWCAD, Patuxent River. Susan Polsky is the technical monitor and provided the wind tunnel data for the cases presented here. Her involvement and guidance are gratefully acknowledged. Valuable discussions with Ryan Czerwiec, also from NAWCAD, and Colin Wilkinson of Anteon Corporation are also gratefully acknowledged.

References

[1] Polsky, S.A. and Bruner, C.W.S., "Time-Accurate Computational Simulations of an LHA Ship," AIAA Paper 2000-4126, June 2000.

[2] Polsky, S.A., "A Computational Study of Unsteady Ship Airwake," AIAA-2002-1022, Jan 2002.

[3] Advani, S. K. and Wilkinson, C. H., "Dynamic Interface Modelling and Simulation – A Unique Challenge," Presented at the Royal Aeronautical Society Conference on Helicopter Flight Simulation, London, November 2001.

[4] Arunajatesan, S., Shipman, J. D. and Sinha, N., "Towards Numerical Modeling of Coupled VSTOL-Ship Airwake Flowfields," AIAA-2004-0052, Jan 2004.

[5] Walker, M. A. and Kimmel, K. R., "Wind Tunnel Investigation of the Unsteady Air Wake Along the Flight Path Behind CVN-73 and CVN-76 Aircraft Carrier Configurations," NSWC Carderock Division Report No. CRDKNSWC/HD-1422-04, April, 1996.

[6] Walker, M. A. and Kimmel, K. R., "Wind Tunnel Flowfield Survey of the Unsteady Air Wake Behind CVN-73 and CVN-76 Aircraft Carrier Configurations," NSWC Carderock Division Report No. CRDKNSWC/HD-1422-05, December, 1997.

[7] Gridgen, Grid Generation Software Package, Version 15, Pointwise, Inc., Ft. Worth, TX, 2004.